Chemical Engineering Journal 452 (2023) 139339

Contents lists available at ScienceDirect

Chemical Engineering Journal

journal homepage: www.elsevier.com/locate/cej

In-situ preparation of gel polymer electrolytes in a fully-assembled lithium ion battery through deeply-penetrating high-energy electron beam irradiation

Seokyoung Park [a,b,1], Joon-Yong Sohn [a,c,1], In-Tae Hwang [a], Junhwa Shin [a], Jin-Mun Yun [a], KwangSup Eom [d], Kwanwoo Shin [b], Young-Moo Lee [c,*], Chan-Hee Jung [a,*]

[a] Advanced Radiation Technology Institute, Korea Atomic Energy Research Institute, 29 Geumgu-gil, Jeongeup, Jeollabuk-do 56212, Republic of Korea
[b] Department of Chemistry & Institute of Biological Interfaces, Sogang University, 35 Baekbeom-ro, Mapo-gu, Seoul 04107, Republic of Korea
[c] Department of Energy Engineering, Hanyang University, 222 Wangsimni-ro, Seongdong-gu, Seoul 04763, Republic of Korea
[d] School of Materials Science and Engineering, Gwangju Institute of Science and Technology (GIST), 123 Cheomdangwagi-ro, Buk-gu, Gwangju 61005, Republic of Korea

ARTICLE INFO

Keywords:
In-situ polymerization
Initiator-free
Electron beam irradiation
Gel polymer electrolyte
Lithium ion battery

ABSTRACT

Several in-situ preparation methods of gel polymer electrolytes (GPEs) to develop long-lasting and safe lithium ion batteries (LIBs) recently have been reported. However, the reported in-situ methods still have technical gaps for practical industrial uses in terms of processing time, integrity with the current production line, and scalability. Here, we report an in-situ method to prepare crosslinked poly(vinylene carbonate-*co*-cyanoethyl acrylate) (PVCEA) GPEs using 10 MeV electron beam (EB) irradiation in a fully-assembled metallic housing LIB that can be processed in a short time without any initiator or thermal treatment. The successful in-situ formation of PVCEA GPEs was achieved at absorbed doses above 16 kGy (irradiation time of 56 s), leading to intimately integrated GPEs with the electrodes, while ensuring stable charge and discharge performance. The prepared PVCEA GPE exhibited a higher transference number (t_{Li+} = ca. 0.53) and a wider electrochemical operation window (up to 5.0 V) than those of a liquid electrolyte (LE), while providing good ionic conductivity (1.17 mS/cm at 20 °C). Furthermore, the PVCEA GPE-based LIB prepared at an optimized dose of 16 kGy showed comparable retention capacity of 83 % at 0.5C to the conventional LE-based LIB after 300 cycles at 25 °C, and more importantly, better cycling durability at elevated temperature of 60 °C in comparison to the LE-based LIB. This study suggests that the combination of radiation-sensitive precursor formulation and high-energy EB with high penetration ability can provide a promising solution for industrial production of high-performing and safe LIBs.

1. Introduction

Lithium-ion batteries (LIBs) are increasingly being applied to large-scale electric storage including electric vehicles, unmanned planes, and smart grids in the past several decades [1–3]. Generally, LIBs are mainly composed of a cathode, an anode, a separator, and electrolyte [4–6]. To date, liquid electrolytes (LEs) have been used in nearly all commercial-available LIBs owing to their high ionic conductivity at room temperature and excellent compatibility with various solid electrodes (originating from high fluidity) [7–9]. However, the safety risk of LEs (related to the use of flammable organic solvents) has become one of the critical issues that must be resolved for further development and applications [10–12]. In order to solve this problem, polymer electrolytes have been extensively studied owing to their prominent advantages of low flammability, excellent processability, high electrochemical stability, good mechanical flexibility, and durability [13–15]. Among these, gel polymer electrolytes (GPEs) (in a form incorporating liquid plasticizers and lithium salts into polymer matrices) have been recognized as one of the most desirable candidates for cost-effective, safe, and long-lasting LIBs [16–18]. The GPEs offer an intriguing combination of liquid and solid electrolyte characteristics such as good ionic conductivity compared to that of solid electrolytes and better mechanical

* Corresponding authors at: Advanced Radiation Technology Institute, Korea Atomic Energy Research Institute, 29 Geumgu-gil, Jeongeup, Jeollabuk-do 56212, Republic of Korea.
E-mail addresses: ymlee@hanyang.ac.kr (Y.-M. Lee), jch@kaeri.re.kr (C.-H. Jung).
[1] Equal contributing authors.

https://doi.org/10.1016/j.cej.2022.139339
Received 11 July 2022; Received in revised form 14 September 2022; Accepted 17 September 2022
Available online 23 September 2022

integrity and safety that cannot be easily achieved in LEs [19,20]. These useful characteristics of the GPEs in LIBs also can be applied to other energy storage devices such as supercapacitors and lithium ion capacitors that have been facing similar problems [21–24].

The preparation of the GPEs (based on polymer physical gelation, chemical polymer crosslinking, and polymerization in the presence of LEs) has been widely conducted by both ex-situ and in-situ approaches [25–28]. An ex-situ approach was attempted by fabricating GPEs externally first and then applying them to the assembly process of LIBs [27]. Typically, gel-forming polymers (*e.g.* poly(ethylene oxide), poly (methyl methacrylate), polyacrylonitrile, poly(vinylidene fluoride) etc.) are fully mixed with appropriate LEs for the preparation of ex-situ GPEs [20,25,29]. However, this approach is limited in terms of practical use in that it is difficult to achieve intimate contact of the internal active materials, which is critical for low interfacial resistance [26,28]. Meanwhile, an in-situ approach was recently proposed to overcome the above-mentioned limitation and take full advantage of the inherent characteristics of GPEs. This in-situ preparation of GPEs by polymerization in a fully-assembled battery state has been implemented mainly by thermal treatment (rather than UV irradiation because UV cannot penetrate the fully-assembled battery to initiate and propagate polymerization) [26,27]. Research on the in-situ preparation of GPEs has been mainly performed through thermal free-radical polymerization and crosslinking using precursor solutions consisting of free-radical initiators, LE, vinyl monomers (*e.g.* acrylate, methacrylate, acrylonitrile, carbonate derivatives, etc.), and multi-functional crosslinkers (e.g. poly(ethylene glycol) diacrylate, trimethylolpropane triacrylate, ethoxylated trimethylopropane triacrylate, pentaerylthritol tetraacrylate, etc.) [27,30–32]. Most of the in-situ GPEs prepared by this method exhibit excellent mechanical properties and stable interfacial compatibility with battery components while retaining the ionic conductivity of LEs [33–35]. However, the thermal process requires processing time of 0.5 ~ 8 h at elevated temperature of 60 ~ 80 °C [30–37]. Furthermore, unwanted side reactions such as the formation of gas bubbles during the thermal process bring about an increment in the internal resistance and considerable polarization, which can decrease the full battery cycling performance [38–40]. As an alternative method to prepare in-situ GPEs, a room temperature ionic polymerization method has been attempted using tri(ethylene glycol) divinyl ether, ethyl cyanoacrylate, tetrahydrofuran, and 1,3-dioxolane [26,41–48]. Although it has been reported that the prepared GPEs show excellent electrochemical properties desirable to realize safe and high performing LIBs, it is also known that controlling the in-situ ionic polymerization for the formation of reliable GPEs is difficult [42,45,48]. Therefore, there is still a high demand for a rapid, room temperature, initiator-free, and cost-effective approach that is, perhaps more importantly, compatible with the existing LIB process currently operated in battery production lines.

The high-throughput and cost-effectiveness of high-energy radiation processing has been extensively established in various industrial polymer-processing fields including heat-resistant wires and cables, radial tires, heat shrinkable tubes and films, battery separators, etc [49]. This processing enables various room-temperature chemical reactions of polymerization, crosslinking, grafting, and degradation, depending on the chemical structure of polymers and irradiation conditions even in the absence of chemical additives (*i.e.* initiator) and/or solvents. In addition, high-energy radiation processing can be applied even for the treatment of thick voluminous products due to its high penetrating power [50–52]. The radiation processing with these many advantages has also been successfully applied for the in-situ preparation of GPEs [53–55]. γ-Rays resulting from the decay of ^{60}Co have higher penetrating power that enables them to pass through thicker substances (up to several tens of centimeters in case of water) while the penetration ability of an electron beam (EB) largely depends on the EB power generated from the accelerator [50]. For example, a 10 MeV high-energy EB can penetrate up to several centimeters in water whereas a 1 MeV EB penetrates less than one centimeter [51]. The in-situ GPEs were successfully prepared in a fully-assembled state by γ-ray irradiation; however, long irradiation time (several hours) and the use of γ-rays may limit industrial application [53,54]. More recently, a study on radiation polymerization in a pouch-type battery via an EB irradiation was reported to demonstrate the advantages of radiation in terms of processing time and effectiveness [55]. In the aforementioned study, although the absorbed dose was used to confirm the gelation of the irradiated GPEs and compare their ionic conductivities, the radiation effects on the in-situ preparation of GPE-based batteries in a fully-assembled state and their cycling performance were not clearly described. In addition, in this study, only the absorbed dose was reported without other essential EB processing information including the EB energy, the beam current, and the scan rate. While the absorbed dose is an important factor to determine reaction progress (gelation in this study) and the resulting properties of the irradiated samples, other factors are important as well. For example, the EB energy determines the penetration depth of the accelerated electrons while the beam current and the scan rate determine the productivity.

The aim of this research was to develop a high-energy EB-induced polymerization method for the preparation of a crosslinked GPE-based LIB in a fully-assembled battery state, compatible with the existing LIB production line. This high-energy EB irradiation strategy included a combination of an EB-sensitive GPE precursor (ensuring physical integrity of GPE without leakage of LE), a nonwoven olefin fabric spacer (reducing the insulating polymer portion while maintaining a physical barrier to avoid undesirable contact between electrodes), and 10 MeV EB-based radical polymerization (penetrating metallic hard battery housing materials) [56–59]. These liquid precursors (consisting of vinylene carbonate (VC), 2-cyanoethyl acrylate (CEA), dipentaerythritol penta-/*hexa*-acrylate (DPTPHA), and liquid electrolyte) and their relative content were optimized in consideration of miscibility, radiation sensitivity, mechanical robustness, and electrochemical stability [60–65]. With this strategy, a flexible free-standing crosslinked poly (vinylene carbonate-*co*-cyanoethyl acrylate) (PVCEA) GPE was successively prepared even in a metallic hard housing coin-type LIB at an absorbed dose of 16 kGy (short irradiation time of less than one minute). It exhibited a higher transference number (t_{Li+} = 0.53 at 25 °C) and a wider electrochemical operation window (up to 5.0 V) than those of the LE reference, while providing ionic conductivity (1.17 mS/cm at 20 °C) comparable to that of the LE reference. Electrochemical impedance spectroscopy (EIS) related to the parasitic reactions imposed by unreacted monomers and/or low molecular weight oligomers confirmed that the minimum absorbed dose of 16 kGy for the high-performing PVCEA GPE-based LIB (consisting of $Ni_{0.2}Co_{0.8}Mn_{0.3}$ (NCM523, loading mass = 12.1 mg/cm^2) cathode and graphite (8 mg/cm^2) anodes) was required in this system. As a result, the PVCEA GPE-based LIB prepared at the minimum dose shows a high capacity of ~ 128 mAh/g and capacity retention of > 80 % at 0.5C after 300 cycles at 25 °C, which are comparable with the capacity of a LE-based LIB with the same electrodes. Notably, regarding the charge–discharge cycling stability at elevated temperature (60 °C), the GPE-based LIB was found to be more durable than LE-based LIBs, demonstrating the better, thermally stable performance of the PVCEA GPE.

2. Experimental

2.1. Materials

Vinylene carbonate (VC, > 98.0 %) and 2-cyanoethyl acrylate (CEA, > 95.0 %) were purchased from Tokyo Chemical Industry (TCI). Dipentaerythritol penta-/*hexa*-acrylate (DPTPHA) was purchased from Merck chemical company. A commercial lithium hexafluorophosphate ($LiPF_6$) solution (1 M $LiPF_6$ in ethylene carbonate (EC)/diethylcarbonate (DEC)/dimethylcarbonate (DMC) = 1/1/1, v/v/v + fluoroethylene carbonate (FEC) 10 wt%) was obtained from Soulbrain and used as a liquid electrolyte (LE). The $LiNi_{0.5}Co_{0.2}Mn_{0.3}O_2$ (NCM523) cathode

(NCM523 electrode coated on aluminum foil, active material proportion: 94.2 wt%, active material density: 12.1 mg/cm^2), graphite anode (mesocarbon microbeads (MCMB) electrode coated on copper foil, active material proportion: 94.5 wt%, active material density: 8 mg/cm^2), polypropylene separator (25 μm, 41 % porosity, Celgard2400), and 2320 coin-battery case were supplied from MTI Korea. A 70 μm-thick nonwoven polyethylene/polypropylene fabric separator (OCP, No. 16, density = 0.188 ± 0.02, tensile strength = 20 MPa) was obtained from Namyang nonwoven fabric. All the chemicals were used as received.

2.2. Preparation of crosslinked PVCEA GPEs by electron beam irradiation

The precursor solutions for PVCEA GPEs were first prepared in an argon-filled glove box by mixing VC monomer, CEA comonomer, and DPTPHA crosslinker in different molar ratios of 28.5:66.5:5 (VC:CEA = 3:7), 47.5:47.5:5 (VC:CEA = 5:5), and 66.5:28.5:5 (VC:CEA = 7:3) while maintaining the ratio of crosslinker at 5 mol%. The resulting solutions were mixed with commercial $LiPF_6$ liquid electrolyte in a fixed 10:90 wt ratio of precursor solution to $LiPF_6$ liquid electrolyte. After filling 4 ml of resulting precursor solutions into 10 ml propylene syringes, the syringes were wrapped with aluminum pouches, and the pouches were thermally sealed to retain the argon atmosphere. To investigate the gelation behavior of the precursor solutions, the sealed aluminum pouches were electron beam (EB)-irradiated at room temperature from a high-energy 10 MeV electron accelerator (Mevex) installed at the Korea Atomic Energy Research Institute (KAERI, Republic of Korea).

The irradiation dose (the corresponding irradiation time) ranged from 4 (14 *sec*) to 20 kGy (70 *sec*) at a fixed rate of 4 kGy/scan (corresponding to 14 *sec*/scan). Radiochromic B3 (BCE 3000 batch) film dosimetry was performed according to ISO/ASTM 5149 with less than 5 % uncertainty. For the characterization of the irradiated samples (in terms of gel fraction, swelling degree, retention rate, thermal decomposition temperature, and compressive strength), the obtained cylindrical PVCEA GPEs (with a diameter of around 12 mm) from the syringe were cut into 10 mm-thick pieces. The prepared GPE samples were denoted as PVCEA(X:Y)-Z, where X:Y and Z stand for the monomer molar ratio and the absorbed dose, respectively.

2.3. Characterization of the PVCEA GPEs

The gel fraction and swelling degree of the PVCEA GPEs were determined by the gravimetric method according to ASTM D2765-01. The gel fraction was evaluated by measuring the weight changes of the dried GPEs before and after extraction in an EC/DEC/DMC solvent at room temperature for 24 h and subsequent drying in a vacuum oven at 80 °C for 24 h. The gel fraction of the samples was calculated by the following equation:

$$\text{Gel fraction}\,(\%) = \frac{W_e}{W_o} \times 100 \tag{1}$$

where W_o and W_e are the weight of the dried GPEs before and after the solvent extraction, respectively.

For measurement of the swelling degree, the GPE samples were immersed in an EC/DEC/DMC solvent. After swelling for 24 h, the samples were gently wiped with soft paper tissue in order to remove the solvent from the surface and then the weights of the wiped samples were measured. The swelling degree of the samples was calculated by the following equation:

$$\text{Swelling degree}\,(\%) = \frac{W_s - W_o}{W_o} \times 100 \tag{2}$$

where W_s is the swollen weight of the GPEs after swelling in an EC/DEC/DMC solvent.

The retention rate of PVCEA GPEs and LE was estimated by measuring the weight changes over time in a glove box at room temperature. The LE retention rate of the samples was calculated by the following equation:

$$\text{LE retention rate}\,(\%) = \frac{W_f}{W_i} \times 100 \tag{3}$$

where W_f is the weight of the GPEs after being stored for a certain time and W_i is the initial weight of the GPEs.

The chemical structure for the PVCEA GPEs was analyzed using attenuated total reflectance Fourier transform infrared spectrometry (ATR-FTIR, 640-IR, Varian). The thermal stability of PVCEA GPEs was investigated using a thermogravimetric analysis (TGA, Q500 analyzer, TA Instrument) under a nitrogen atmosphere at a heating rate of 10 °C/min in the range of 30 ~ 500 °C. The compressive strength and strain of 10 mm-diameter PVCEA GPEs were measured using a universal testing machine (UTM, TA-XT2i texture meter, Surrey) at a compressive rate of 5 mm/min.

2.4. In-situ formation and characterization of PVCEA GPEs in fully-assembled coin-type battery

All electrochemical evaluations of the prepared GPE battery (hard housing 2032 coin type) were conducted after assembling the battery components including radiation-sensitive GPE precursors in the glove box followed by irradiation with a 10 MeV electron accelerator. The nonwoven fabric (OCP) was used as a separator to prevent direct contact between two electrodes and to retain the liquid precursors. Ionic conductivities were determined using electrochemical impedance spectroscopy (EIS) with symmetric coin cells (stainless steel (SS, ϕ = 16 mm)/GPE(OCP)/SS). For comparison, SS/LE(OCP) or LE(Celgard)/SS batteries were prepared by using LE with OCP or Celgard, respectively. EIS spectra were recorded on a multichannel electrochemical workstation (ZIVE MP1, ZIVE LAB) with a potential amplitude of 10 mV and frequencies from 1 MHz to 0.1 Hz at a temperature range from 0 to 60 °C. The ionic conductivity of the batteries was calculated through the following equation:

$$\sigma = \frac{t}{(R \times A)} \tag{4}$$

where t is the thickness of the PVCEA GPE, R is the measured bulk resistance, and A is the contact area between the GPE and SS. Linear sweep voltammetry (LSV) for the electrochemical oxidation stability of the PVCEA GPEs was performed by using an electrochemical analyzer (VersaSTAT4, AMETEK Inc.). The LSV curve was obtained using asymmetric batteries of SS/GPE(OCP)/Li and SS/LE(OCP)/Li in a voltage range of 0 to 6 V under a scanning rate of 5 mV/s. For measurement of the lithium ion transference number (t_{Li+}), EIS and DC polarization of symmetric batteries of Li/LE(OCP)/Li and Li/PVCEA(5:5)-16 GPE (OCP)/Li were tested, and t_{Li+} was calculated according to the following Bruce-Vincent-Evans equation:

$$t_{Li+} = \frac{I_s(\Delta V - I_0 R_0)}{I_0(\Delta V - I_s R_s)} \tag{5}$$

where I_0 is the initial current before polarization, I_s is the steady-state current, $\triangle V$ is the applied polarization voltage of 10 mA, and R_0 and R_s are the initial and steady-state interfacial resistances of the passivation layers on the Li electrode, respectively.

For morphological and chemical composition observation, as well as a full battery test of in-situ PVCEA GPEs-based LIBs, the batteries were fully assembled by adding 200 μL of as-prepared precursor (at the VC:CEA molar ratio of 5:5) into the nonwoven fabric OCP between NCM523 and graphite electrodes and clamping. After resting for 10 h to fully wet the electrodes with the precursors, the fully-assembled batteries were exposed to an EB at absorbed doses of 4, 8, 16, and 20 kGy. For the sake of comparison, the same assembly procedure was applied for the

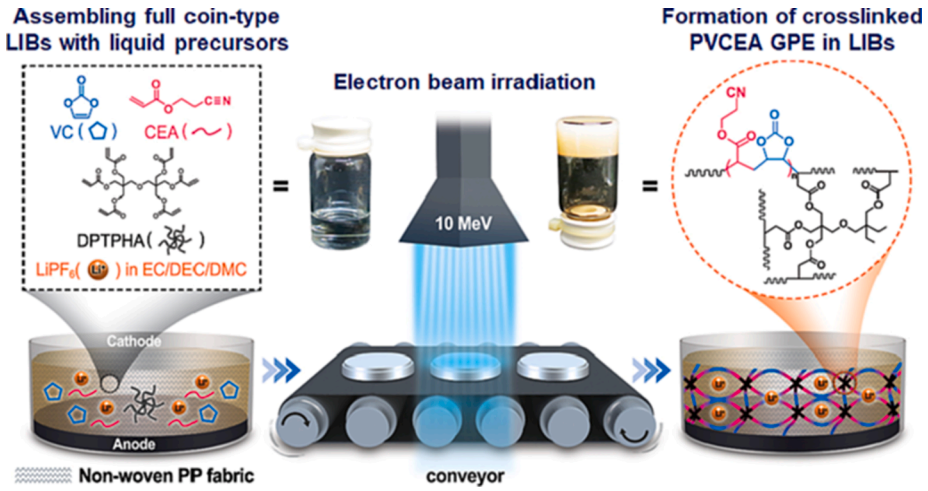

Fig. 1. Schematic illustration for the in-situ fabrication of crosslinked PVCEA GPEs-based LIBs by electron beam irradiation in a fully-assembled metallic housing battery state (inset shows the chemicals used in the precursor solutions and the crosslinked structure of the resulting GPEs).

Table 1
Precusor formulation and absorbed dose for in-situ fabrication of crosslinked PVCEA GPEs-based LIBs.

Samples	Liquid precursor composition				Separator	Abosrbed dose (kGy)
	Radiation-sensitive component (wt%)			Liquid electrolyte (wt%)		
	VC (mol%)	CEA (mol%)	DPTPHA (mol%)			
	[VC:CEA] molar ratio					
VC/CEA(5:5)	10		5	90	–	0
	47.5	47.5				
	5:5					
PVCEA(5:5)-4, −8, −16, and −20	10		5	90	OCP	4 ~ 20
	47.5	47.5				
	5:5					
PVCEA(3:7)-16	10		5	90	OCP	16
	28.5	66.5				
	3:7					
PVCEA(7:3)-16	10		5	90	OCP	16
	66.5	28.5				
	7:3					
LE(OCP)		–		100	OCP	–
LE(Celgard)		–		100	Celgard2400	–

preparation of the NCM523/LE(OCP)/graphite and NCM523/LE(Celgard)/graphite batteries. Analysis of the surface morphology and elemental mapping of nonwoven fabric OCP and free standing PVCEA (5:5)-16 (independently prepared in an assembled state without electrodes) were carried out by using a field emission scanning electron microscope (FE-SEM, SU8230, Hitachi) equipped with an energy dispersive X-ray spectroscope (EDS). The cross-sectional morphology and elemental mapping of the pure NCM523 cathode, pure graphite anode, and NCM523/PVCEA(5:5)-16/graphite (taken from the battery) were analyzed by FE-SEM with EDS after freeze-fracturing the samples followed by polishing with ion milling (JEOL, IB-19520CCP).

To determine the minimum absorbed dose, the changes in galvanostatic charging/discharging and impedance of NCM523/PVCEA(5:5) GPEs/graphite batteries (prepared at different absorbed doses) after the 1st and 100th cycles at 25 °C were analyzed by using a battery charge/discharge test system (WBCS3000L, Won A Tech) under a rate of 0.5C (1C = 1.876 mA/cm^2) between 3.0 and 4.2 V at 25 °C and EIS, respectively. The rate capability of NCM523/PVCEA(5:5)-16/graphite and reference batteries with LE(OCP) or LE(Celgard) was assessed by using a charge/discharge test system under different rates of 0.2, 0.33, 0.5, 1.0, 1.5, and 2C at 25 °C. Cycling performance of NCM523/PVCEA (5:5)-16/graphite and the reference battery with LE(OCP) was evaluated by using the charge/discharge test system under a rate of 0.5C at 25 and 60 °C.

3. Results and discussion

The in-situ formation of the crosslinked poly(vinylene carbonate-*co*-2-cyanoethyl acrylate) (PVCEA)-based GPEs by EB irradiation in a fully-assembled coin-type battery state is illustrated in Fig. 1. To obtain the radiation-sensitive liquid precursor solutions, vinylene carbonate (VC), 2-cyanoethyl acrylate (CEA), and dipentaerythritol penta-/*hexa*-acrylate (DPTPHA) were mixed together according to the molar ratio in Table 1 followed by additional mixing with $LiPF_6$ liquid electrolyte (LE) (where the weight ratio of the VC/CEA/DPTPHA mixture to the LE was fixed to 10:90). The resulting precursor solutions were subsequently injected into the nonwoven fabric (OCP) separator between the cathodes and anodes. In this study, a less dense nonwoven fabric was used as a separator instead of a relatively dense conventional olefin separator since it is capable of reducing the insulating portion while maintaining a physical barrier between electrodes, and it also can hold a large amount of GPE precursor solution [66,67]. To in-situ create robust and high-performing GPEs without long thermal treatment and an inert atmosphere, a fully-assembled battery containing the GPE precursor solution

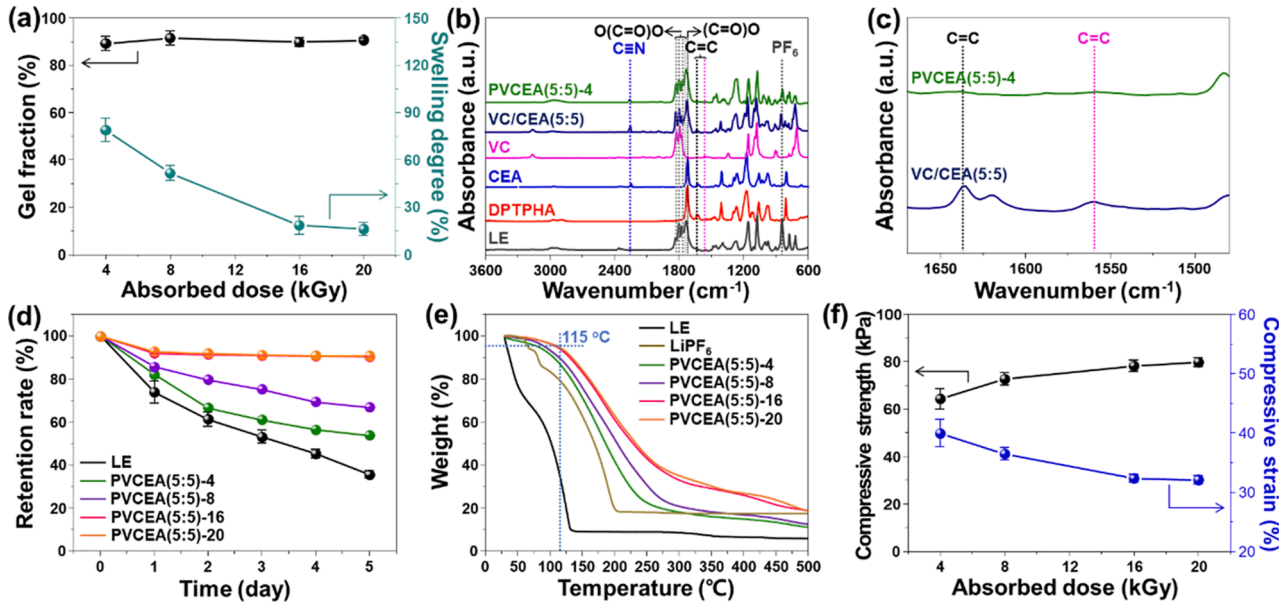

Fig. 2. Structural and physico-chemical properties of the PVCEA GPEs: (a) Gel fraction and swelling degree of PVCEA(5:5) GPEs as a function of absorbed dose; (b) ATR-FTIR spectra of LE, DPTPHA, VC, CEA, VC/CEA(5:5), and PVCEA(5:5)-4; (c) ATR-FTIR spectra of VC/CEA(5:5) and PVCEA(5:5)-4 in the wavenumber between 1670 cm^{-1} and 1480 cm^{-1}; (d) Retention rate of LE, PVCEA(5:5)-4, −8, −16, and −20; (e) TGA curves of LE, PVCEA(5:5)-4, −8, −16, and −20; (f) Compressive strength and strain of LE, PVCEA(5:5)-4, −8, −16, and −20.

was subjected to 10 MeV EB irradiation at room temperature. During the irradiation, the reactive radicals from the double-bond dissociations of radiation-sensitive components initiate polymerization to form a crosslinked PVCEA matrix firmly holding the liquid electrolytes [60]. In order to observe the penetrating power of the 10 MeV EB into the fully-assembled coin battery, radiochromic B3 dosimetry films were attached to the top and bottom of the coin battery and their color changes after EB irradiation (16 kGy) were analyzed according to ISO/ASTM 51,649 to measure the absorbed doses (Fig. S1). The measured absorbed doses of the irradiated films attached to the top and bottom (measured using a Spectronic Genesys 2 UV–vis spectrophotometer (Thermo Fisher Scientific, USA)) were 15.4 kGy and 16.3 kGy, respectively, within an error range of less than 4 % of the set dose. These results clearly demonstrate that 10 MeV EB can penetrate the fully-assembled metal housing coin battery without recognizable energy loss under the given conditions of this study. To verify possible radiation damage on the electrodes and liquid electrolyte arising from high-energy EB irradiation (Fig. S2), the NCM523/graphite battery with LE(OCP) irradiated at an absorbed dose of 50 kGy showed capacity retention of 96 % at 0.5C after 50 cycles at 25 °C, almost identical to that of the non-irradiated battery (97 %). This suggests that crosslinked PVCEA GPE can be prepared without meaningful detrimental damage to the electrolytes and electrodes. Moreover, the insets in Fig. 1 show that the irradiated precursor solution at an absorbed dose of 4 kGy was clearly converted into non-fluidic PVCEA GPEs desirable for the safety of LIBs, even containing 90 wt% LE. In comparison with thermal radical and ionic polymerization approaches, this strategy offers discernible advantages of rapid and room-temperature processing and, more importantly, excellent compatibility with the current LIB manufacturing line.

3.1. Formation and characterization of crosslinked PVCEA GPEs

It is well known that the absorbed dose is a critical factor in radiolytic polymerization and crosslinking [68,69]. To investigate the effect of the absorbed dose on the formation of PVCEA GPEs, the gel fraction and swelling degree, which critically influence the liquid electrolyte (LE) retention, thermal stability, and mechanical robustness of the GPEs, were measured after EB irradiation of the precursor solutions with a fixed VC:CEA molar ratio of 5:5 at absorbed doses of 4, 8, 12, 16, and 20 kGy. As shown in Fig. 2(a), all the PVCEA GPEs exhibited similar gel fractions of around 90 % at the given absorbed doses, indicating that the GPEs were effectively formed even from the precursor solution containing 90 % of $LiPF_6$ LE at absorbed doses above 4 kGy. On the other hand, the swelling degree of the PVCEA(5:5) GPEs was markedly decreased up to 16 % as the absorbed dose was increased to 16 kGy, and appeared to converge at a higher absorbed dose. This indicates that a denser crosslinked structure, assuring greater dimensional stability, can be introduced in the GPEs at absorbed doses above 16 kGy.

Table 2
Main characteristic ATR-FTIR bands (cm^{-1}) of LE, DPTPHA, VC, CEA, PVCEA (5:5)-0, and PVCEA(5:5)-4 in Fig. 2(b) and (c).

	LE	DPTPHA	CEA	VC	VC/CEA (5:5)	PVCEA (5:5)-4
C≡N			2251		2251	2251
O(C═O)O (VC)				1824	1828	1832
O(C═O)O (EC)	1801, 1774			1791, 1776	1795, 1774	1803, 1774
O(C═O)O (DEC)	1734					1738
(C═O)O (DPTPHA & CEA)		1720	1724		1724	
C═C (VC)				1560	1560	
C═C (DPTPHA & CEA)		1620	1620		1619	
PF_6	843				846	840

To provide the chemical structure information of the prepared PVCEA GPEs from the precursor solutions by EB irradiation, an ATR-FTIR analysis was performed with the PVCEA(5:5)-4 GPE prepared at absorbed does of 4 kGy. As shown in Fig. 2(b) and Table 2, the spectrum of the VC/CEA(5:5) as a liquid precursor showed the characteristic bands at 2251 cm^{-1} (C≡N in CEA), 1810 ~ 1720 cm^{-1} (O(C═O)O in EC/DEC/DMC and O(C═O)O in VC), 1620 cm^{-1} (C═C in CEA and C═C

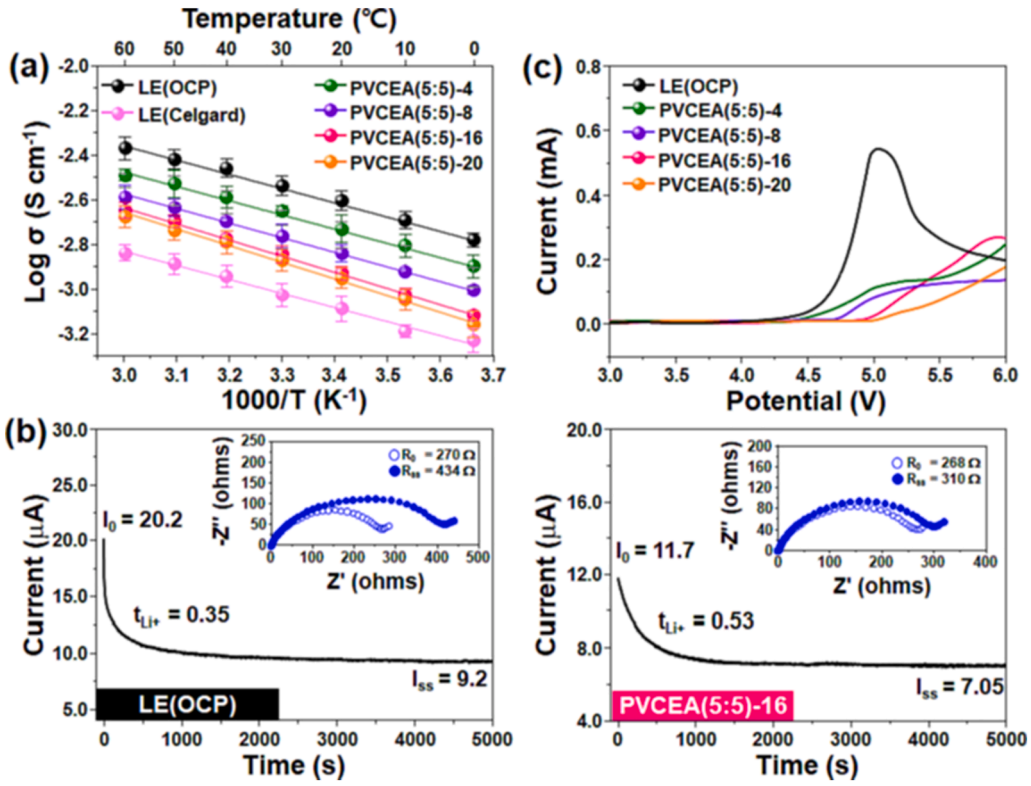

Fig. 3. Electrochemical properties of the PVCEA GPEs: (a) Arrhenius ionic conductivity plots of LE(OCP16), LE (Celgard), PVCEA(5:5)-4, −8, −16, and −20; (b) Current-time profiles of Li/Li symmetric batteries with LE(OCP 16) and PVCEA(5:5)-16 polarized at a dc voltage of 10 mV (the insets in each profile show the Nyquist impedance spectra of the batteries before and after polarization); (c) Linear sweep voltammetry curves of LE(OCP16), PVCEA (5:5)-4, −8, −16, and −20 at a scanning rate of 5 mV/s.

in DPTPHA), 1560 cm^{-1} (C═C in VC), and 846 cm^{-1} (P-F in $LiPF_6$), corresponding to the spectra of VC, CEA, DPTPHA, and LE [70–73]. The bands, indicative of the ester of CEA and DPTPHA at 1720 cm^{-1} in the spectrum of VC/CEA(5:5), cannot be discriminated because they overlap those of the EC/DEC/DMC in the LE spectrum. In the spectrum of PVCEA (5:5)-4 (Fig. 2(c) and Table 2), the most characteristic bands of the CEA VC, CEA, DPTPHA, and LE (present in the VC/CEA(5:5) spectrum) identically appeared except for the C═C bands. The C═C bands clearly disappeared at 1620 cm^{-1} (C═C in CEA or C═C in DPTPHA) and 1560 cm^{-1} (C═C in VC))]. These results strongly support that the radiation-sensitive VC, CEA, and DPTPHA were effectively polymerized in the presence of the LE even under the given absorbed dose of 4 kGy, resulting in crosslinked PVCEA GPEs.

To assess important features essential for the safety performance of the integrated LIBs including the LE retention capability, thermal stability, and mechanical robustness, PVCEA(5:5) GPEs prepared at different absorbed doses were analyzed by retention rate measurement, TGA, and UTM. As shown in Fig. 2(d), the retention rate of LE rapidly decreased, and was only 36 % after five days. On the other hand, the PVCEA(5:5) GPEs exhibited a higher retention rate than the LE at the given times, and the retention rates were dependent on the absorbed dose due to the difference in the crosslinking density, as mentioned in relation to the swelling degree [74–76]. In particular, both PVCEA(5:5)-16 and −20 GPEs (prepared at absorbed doses above 16 kGy) showed excellent retention rates of 91 % even after five days. From this result, it can be inferred that the PVCEA(5:5) GPEs produced at absorbed doses above 16 kGy can effectively suppress the evaporation of LE because of the formation of a denser crosslinked structure. As shown in the TGA curve of the LE (Fig. 2(e)), two main weight losses occurred within the temperature ranges of 30 – 80 ℃ (corresponding to volatilization of EC/DEC/DMC solvent) and 75 – 150 ℃ (attributed to the decomposition of $LiPF_6$) [54]. On the other hand, the weight loss of all the PVCEA(5:5) GPEs was initiated at higher temperature of over 85 ℃ in comparison to weight loss of liquid electrolyte and $LiPF_6$. This indicates that the solvent and $LiPF_6$ exist more stably in the crosslinked PVCEA gel, likely due to the interaction with the functional groups of PVCEA chains and the low mobility in the gel state [54,60,77]. In particular, the initial decomposition temperatures of the PVCEA(5:5)-16 and −20 (corresponding to the less than the weight loss of 5 %) were measured to be around 115 ℃ (higher than those prepared at the lower absorbed doses). This better thermal stability is also ascribed to the formation of the denser crosslinked structure into the PVCEA(5:5) GPEs at absorbed doses above 16 kGy. As shown in Fig. 2(f), the compressive strengths of the PVCEA(5:5) GPEs were gradually increased with increasing absorbed dose, whereas the compressive strains decreased. Among these, the PVCEA(5:5)-16 and −20 exhibited higher compressive strengths of 78.1 kPa and 79.7 kPa, respectively. Overall, GPEs with a robust PVCEA(5:5) that hold LE better and are thermally stable can be produced at absorbed doses above 16 kGy (corresponding to irradiation time of only 56 s). In addition, it is worth noting that the characteristics of PVCEA GPEs can be easily controlled by the absorbed dose. This can be explained by the fact that the crosslinked PVCEA GPEs are created in a chemically-integrated state from the homogenous liquid precursors of radiation-sensitive components, $LiPF_6$, and EC/DEC/DMCs, unlike the conventional physical gel system (fabricated by soaking solid polymer matrices with LE) [25].

3.2. *Electrochemical properties of PVCEA GPEs*

The electrochemical properties of the PVCEA GPEs prepared at different absorbed doses were analyzed in terms of ionic conductivity, ion transference, and electrochemical stability. These analytic methods are essential to evaluate the electrochemical performance of the prepared GPEs in the LIBs [20]. For a comparison study, LE(OCP) was used as a counterpart reference of the PVCEA(5:5) GPEs. In particular, for the ionic conductivity measurement, LE(Celgard) was also used for the comparative assessment. As shown in the Arrhenius ionic conductivity plots (Fig. 3(a)), LE(OCP) in this system exhibited higher ionic conductivity (σ) of 2.48 mS/cm at 20 ℃ than LE(Celgard) with σ of 0.81 mS/cm. This result indicates that the nonwoven fabric OCP (density = 0.188 ± 0.02) with a pore size of several hundred micrometers can

Table 3
Calculated activation energy (E_a) for the ionic conductivity of LE(OCP), LE (Celgrard), and PVCEA GPEs prepared at different absorbed doses.

Electrolytes	E_a (kJ/mol)	R^2
LE(OCP)	12.21	0.998
LE(Celgard)	12.00	0.991
PVCEA(5:5)-4	12.22	0.998
PVCEA(5:5)-8	12.58	0.999
PVCEA(5:5)-16	13.97	0.998
PVCEA(5:5)-20	14.29	0.996

provide much larger volume to accommodate LE in comparison to that of the conventional Celgard separator (porosity = 41 %) with a pore size of several dozen nanometers, as presented in the FE-SEM morphologies (Fig. S3) [76]. In the case of the PVCEA(5:5) GPEs, the ionic conductivities (σ) were found to be dose-dependent with variation from 1.85 to 1.11 mS/cm at 20 ℃. This dose dependency can be explained by the fact that the incorporation of the crosslinked polymer matrix impedes the ionic transport in the GPEs, which is further intensified by the formation of a denser crosslinked structure with an increment in the absorbed dose [75]. More importantly, the ion conductivities (σ) of all the PVCEA GPEs are still higher than that of the LE (Celgard), likely because the PVCEA (5:5) GPEs (formed in the presence of the nonwoven fabric OCP) possess larger occupying ionic transport volume than the LE(Celgard) despite their highly crosslinked structures [67,78,79]. The LE(OCP), LE(Celgard), and all the PVCEA(5:5) GPEs exhibited a linear relationship between log σ and reciprocal temperature following the Arrhenius equation of $\sigma = A \times \exp(-E_a/RT)$, where A is the pre-exponential factor and E_a is the activation energy [71]. As shown in Table 3, the calculated E_a of PVCEA(5:5) GPEs from the linear slope, related to the mobility of carriers, was slightly increased from 12.22 to 14.29 kJ/mol with an increase in the absorbed dose due to the formation of the denser crosslinked structure, as mentioned above. However, the difference in the E_a values between the PVCEA(5:5) GPEs and the LE references (LE(OCP) ($E_a = 12.20$ kJ/mol) and LE(Celgard) ($E_a = 12.00$ kJ/mol)) appeared not to be significant. This indicates that the ionic conduction mechanism in the PVCEA(5:5) GPEs likely follows a solvent diffusion mechanism inside the polymer network with low activation energy, as reported for pure LE, rather than a polymeric segmental motion process with high activation energy [74,80].

The lithium ion transference number (t_{Li+}) was obtained by combining chronoamperometry and AC impedance analysis, where PVCEA(5:5)-16 as a representative sample and LE(OCP) as a reference were used, respectively. As shown in Fig. 3(b), the lithium ion transference number of the liquid electrolyte was measured to be 0.35, similar to that of the conventional LEs reported in the literature [60,79]. On the other hand, the PVCEA(5:5)-16 exhibited a much higher lithium ion transference number of 0.53, indicating that the PVCEA GPEs can efficiently diminish the concentration gradient at the electrode surface for better performance of LIBs in comparison to that of the LE [81]. This higher lithium ion transference number of the PVCEA GPE can be reasonably explained as follows [81,82]. The highly-delocalized Lewis basic functionalties of O(C═O)O and C≡N in the crosslinked PVCEA GPE are loosely coordinated with Li^+ ions; this facilitates Li^+ ion transport, resulting in an increase in the number of Li^+ ions. Meanwhile, the migration of anions is suppressed by an electrostatic repulsion effect. As seen in the oxidation stability determined by a linear sweep voltage analysis (Fig. 3(c)), all the PVCEA GPEs exhibited a higher oxidation potential ranging from 4.3 to 5.1 V in comparison to LE(OCP) (4.2 V). In particular, PVCEA(5:5)-16 and PVCEA(5:5)-20 showed excellent oxidation potential above 5 V. This improved oxidation potential is due to the formation of the denser crosslinked structure at higher absorbed dose, which restricts oxidative decomposition of the anions and organic solvents [82,83]. Therefore, it is confirmed from these overall analytic results that the homogenous liquid precursor solution of radiation-sensitive components, $LiPF_6$, and EC/DEC/DMCs was sucessfully converted to thermally-stable and robust crosslinked PVCEA GPEs in a chemically-integrated state by room-temperature EB irradiation without any initiators. In particular, in terms of ionic conductivity, ion transference number, and electrochemical stability, the crosslinked PVCEA GPEs overwhelm the conventional LE with a Celgard separator. Overall, taking into consideration the analytical results of the PVCEA GPEs prepared at the absorbed dose as well as the results of the VC:CEA molar ratio effect (Fig. S4), the VC:CEA molar ratio of 5:5 was selected for further study on the in-situ formation of PVCEA GPEs in a fully-assembled coin battery.

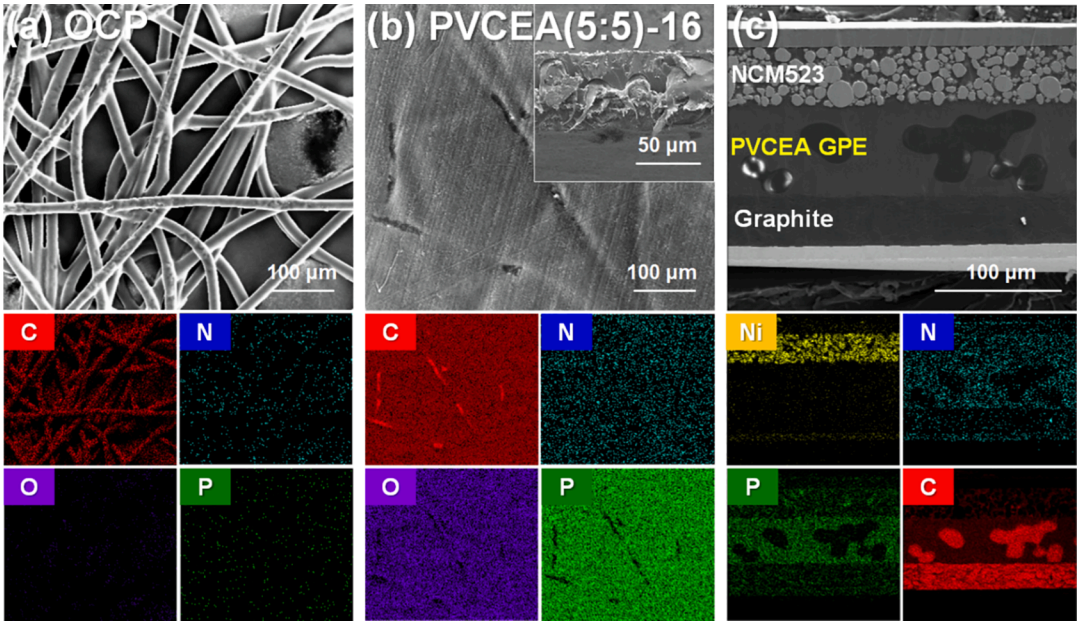

Fig. 4. Morphological observation for the in-situ formation of the PVCEA GPEs in a fully-assembled coin-type battery: FE-SEM images and corresponding EDS mapping of (a) OCP and (b) PVCEA(5:5)-16 GPE independently prepared in an assembled coin-type state without electrodes (Inset in PVCEA(5:5)-16 image shows the corresponding cross-sectional image at × 400 magnification); (c) FE-SEM cross-sectional image and corresponding EDS mapping images of in-situ NCM523/graphite full coin-type battery based on PVCEA(5:5)-16.

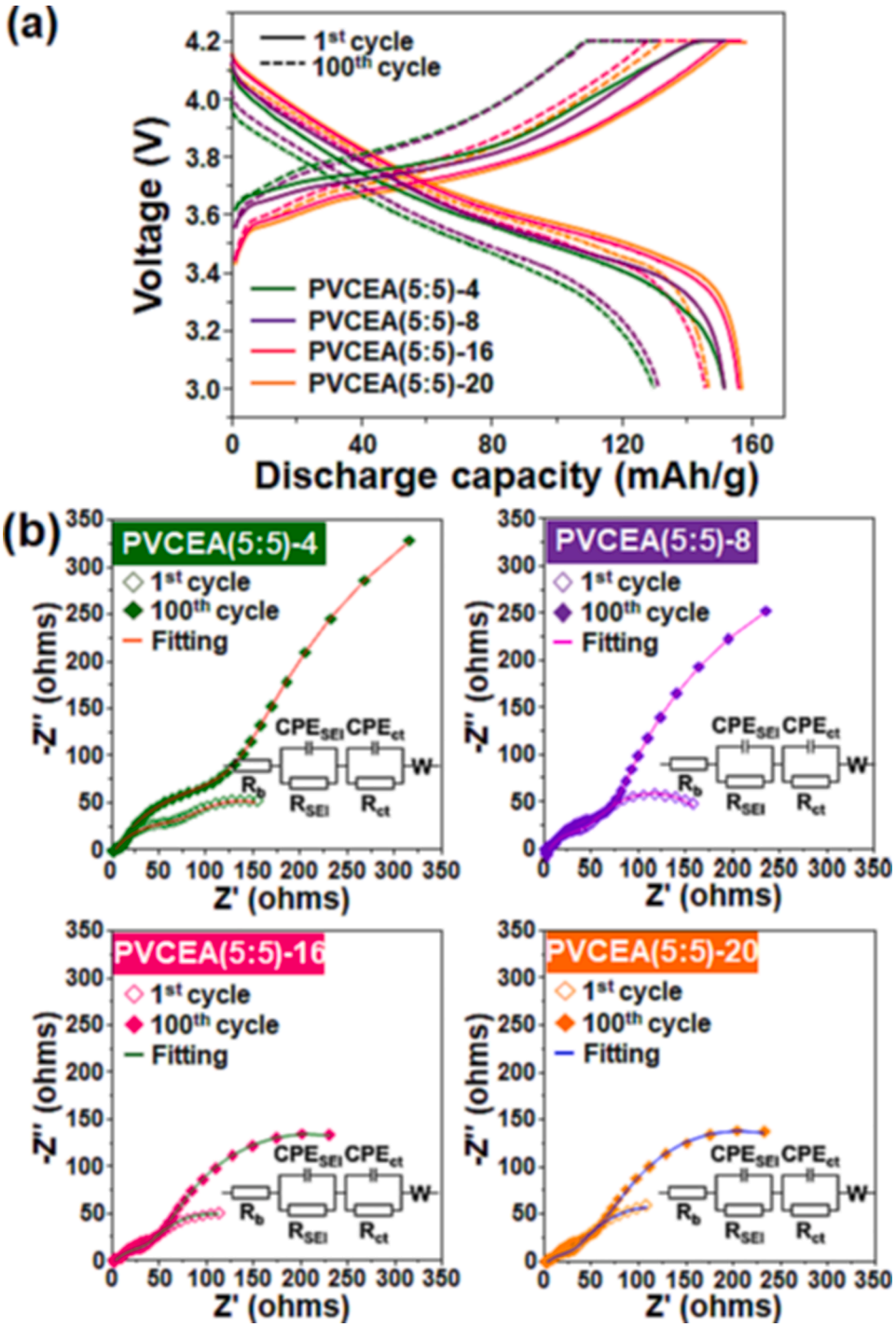

Fig. 5. Charge-discharge performance of in-situ NCM523/graphite full coin-type batteries based on PVCEA(5:5)-4, −8, −16, and −20: (a) Charge-discharge profiles under a rate of 0.5C; (b) Impedance spectra of the batteries after the 1st and 100th cycles (the insets in each spectrum show the corresponding equivalent circuits).

3.3. In-situ fabrication and battery performance of crosslinked PVCEA GPEs in a full coin-type battery

To confirm the in-situ formation of fully-integrated PVCEA GPEs assembled with the NCM523 cathode and graphite anode in a coin-type battery through EB irradiation, the morphology and elemental compositions of PVCEA(5:5)-16 GPE (Fig. S5 (a)) and the in-situ PVCEA(5:5)-16-based NCM/graphite full coin-type battery were observed by a FE-SEM equipped with EDS. As shown in the FE-SEM image of the OCP used as a separator in this study (Fig. 4(a)), the nonwoven fabric OCP exhibited a typical porous structure consisting of randomly entangled fibers. On the other hand, the FE-SEM image of the PVCEA(5:5)-16 (Fig. 4(b)) exhibited a smooth pore-free surface with a morphology of embedded tangled fibers (OCP), while the inset of Fig. 4(b) for the corresponding cross-section of PVCEA(5:5)-16 showed a 70 μm-thick GPE containing relatively brighter round-shape fibers (OCP). In the EDS mapping images of OCP (Fig. 4(a)), the nonwoven fabric only showed the distribution of carbon (C) atoms within the entangled PP/PE fibers. However, in the EDS mapping image of PVCEA(5:5)-16 (Fig. 4(b)), four main elements (consisting of the prepared GPE, carbon (C) (for both OCP and PVCEA), nitrogen (N) for (nitrile group of PVCEA), oxygen (O) (for carbonate and ester groups of PVCEA), and phosphorus (P) atoms

Table 4
Equivalent fitting results of R_b, R_{SEI}, and R_{ct} for impedance spectra shown in Fig. 5(b).

Electrolyte	Cycle	R_b(Ω)	R_{SEI}(Ω)	R_{ct} (Ω)
PVCEA(5:5)-4	1st	4.66	80.25	111.92
	100th	6.95	140.88	901.08
PVCEA(5:5)-8	1st	3.91	66.01	104.05
	100th	6.06	95.70	865.75
PVCEA(5:5)-16	1st	2.87	41.35	177.59
	100th	3.70	72.81	277.09
PVCEA(5:5)-20	1st	3.36	41.30	153.34
	100th	4.15	69.44	283.12

(for $LiPF_6$)) were evenly distributed. In particular, the observed brighter carbon-rich regions in the C mapping image and the darker phosphorus-absent regions in the P mapping are consistent with the morphology of the embedded fibers. This indicates that the PVCEA GPE was well prepared within the entangled fibers of the nonwoven fabric OCP in the fully-assembled metallic hard housing battery state by 10 MeV EB irradiation at an absorbed dose of 16 kGy. In addition, in the FE-SEM image for the in-situ formation of PVCEA in a fully-assembled battery state (Fig. 4(c)), a separated layered structure (consisting of a 48 μm-thick NCM523 cathode as a top layer, a 70 μm-thick PVCEA GPE as a middle layer, and a 45 μm-thick graphite anode as a bottom layer) was clearly observed. It was also found that the surfaces of the cathode and anode layers were very smooth, unlike the rough porous morphologies of pure NCM523 and graphite electrodes (Figs. S5(b) and (c)). Moreover, as shown in the EDS mapping images (Fig. 4(c)), the nickel (Ni) atoms were only distributed in the NCM523 cathode, whereas the C atoms were found in all layered regions. The strong signals of the C atom arise from the carbon-rich graphite and fiber regions, and the relatively weak signals arise from the formed PVCEA GPE and binder. The P and N atoms present in $LiPF_6$ and PVCEA, respectively, (absent in the pure NCM523 and graphite (Figs. S5(b) and (c)) also appeared not only in the PVCEA GPE layer but also in the two electrode layers. These results indicate that the radiation-sensitive precursors (with excellent wettability and fluidity similar to LE) can penetrate the electrodes, and thereby are in-situ converted to the intimately-integrated cross-linked PVCEA GPE with both electrodes by EB irradiation in a fully-assembled battery state. This provides a well-defined ion transporting pathway for low interfacial impedance despite being in a gel state [84,85].

In order to determine the minimum absorbed dose for in-situ formation of PVCEA GPEs in the coin batteries assembled with NCM523 and graphite electrodes, the charge and discharge capacities of the batteries with the in-situ formed PVCEA GPEs at different absorbed doses were measured after the 1st and 100th cycles, and the batteries after the 1st and 100th cycles were analyzed at the same time by using electrochemical impedance spectroscopy (EIS). As shown in Fig. 5 (a), the discharge capacities of PVCEA(5:5)-4 and −8-based batteries both were around 152 mAh/g after the 1st cycle and around 130 mAh/g after the 100th cycle. On the other hand, the PVCEA(5:5)-16 and −20-based batteries both showed higher discharge capacities of around 157 mAh/g after the 1st cycle, and around 146 mAh/g even after the 100th cycle in comparison to that of the PVCEA(5:5)-4 or −8-based batteries. These results indicate that the capacity fading of the PVCEA(5:5)-16 and 20-based batteries are markedly lower than that of the PVCEA(5:5)-4 or −8-based batteries. As shown in the Nyquist plots and the fitting data for the investigation into this absorbed dose-dependent discharge capacity (Fig. 5(b)), the experimental and simulated spectra closely matched, and the corresponding equivalent circuits include bulk resistance (R_b), solid electrolyte interphase resistance (R_{SEI}), and charge transfer resistance (R_{ct}) [82]. As summarized in the simulation results (Table 4), the PVCEA (5:5)-4 and −8-based batteries exhibited significant increases in R_{SEI} and R_{ct} after the 100th cycle without a marked increase in R_b. This increased impedance can be ascribed to the parasite effect of unreacted monomers or oligomers with low molecular weight (unfavorable for stable interfaces between electrodes and electrolyte) [31,86]. However, in the case of the PVCEA(5:5)-16 and 20-based batteries, the increment in R_{SEI} and R_{ct} was not very significant, and the change in R_b was similar to that of the PVCEA(5:5)-4 and −8-based batteries. These results suggest that the PVCEA(5:5) GPEs can be efficaciously in-situ created in the battery at absorbed doses above 16 kGy, thereby leading to the formation of a stable and effective electrode/electrolyte interface with less resistance, resulting in improved performance.

To practically demonstrate the feasibility of in-situ PVCEA-GPE-based LIBs, the in-situ NCM523/PVCEA(5:5)-16/graphite battery was

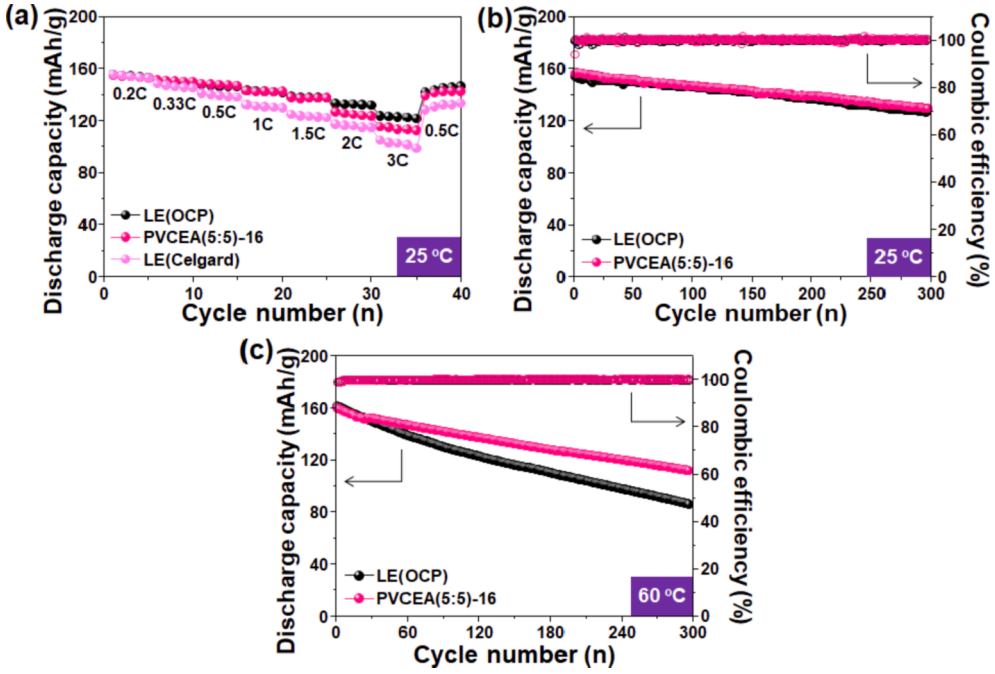

Fig. 6. Performance of in-situ NCM523/graphite full coin-type batteries based on PVCEA(5:5)-16: (a) Rate capability as compared to those with LE(OCP) and LE (Celgard) at 25 °C; Cycling performance as compared to those with LE(OCP) under a rate of 0.5C at (b) 25 and (c) 60 °C.

analyzed in terms of charge–discharge rate and long-term cycling characteristic (Fig. 6). In this study, LE(OCP) and LE(Celgard)-based NCM523/graphite batteries were used for a comparative assessment of the C-rate, and NCM523/LE (OCP)/graphite was used as a counterpart reference for the comparison of long-term cycling characteristic. As shown in the comparison results for the rate capability (Fig. 6(a)), the PVCEA(5:5)-16-based battery delivered reversible capacities of 154.8 (0.2C), 151.1 (0.33C), 148.3 (0.5C), 142.9 (1.0C), and 138.1 mAh/g (1.5C), respectively, almost identical to those of the LE(OCP)-based battery. At higher rates of 2 and 3C, reversible capacities of 127.0 and 115.4 mAh/g were delivered, respectively, which are lower than those of the LE(OCP)-based battery. ATHowever, these reversible capacities of the PVCEA(5:5)-16-based battery at rates above 0.33C were higher than those of the corresponding LE(Celgard)-based battery. This strongly suggests that the PVCEA(5:5) GPEs in-situ formed at the absorbed dose of 16 kGy enables rapid ion transfer at a higher rate than that of LE (Celgard) [67,79]. Even when the rate returned to 0.5C, high capacity of 138.9 mAh/g was retained (similar to the LE(OCP)-based battery and higher than that of LE(Celgard)-based battery). This result is likely attributable to the formation of a stable and effective electrode/electrolyte interface with low resistance caused by the evenly and fully-filled formation of PVCEA GPEs into the cathode and anode electrodes for better contact between the electrolyte and electrodes, as discussed in the results from FE-SEM and EDS [60,84,85].

To estimate the long-term usability (critical for the LIBs), the cycling performance of an in-situ PVCEA GPE-based battery was tested and compared with a LE(OCP)-based battery. As shown in Fig. 6(b), the PVCEA(5:5)-16-based battery delivered a discharge capacity of 129.2 mAh/g after 300 cycles, corresponding to capacity retention of about 83 % with an overall high Coulombic efficiency of 98 %. This cycling performance was comparable to that of the LE(OCP)-based battery with capacity of 127.1 mAh/g corresponding to retention of about 83 % with an overall high Coulombic efficiency of 98 %. The cycling performance test was carried out up to 300 cycles since it is meaningless to draw comparisons in a long-term cycling test up to 500 cycles due to the cycling tolerant limit (retention of 80 % after 500 cycles at 0.2C) of the commercially available cathode used in this study. More importantly, as shown in the cycling capability at elevated temperature (Fig. 6(c)), the PVCEA(5:5)-16-based battery exhibited overwhelmingly better cycling performance at an elevated temperature of 60 ℃ in comparison to that of the LE(OCP)-based battery, verifying the more thermally durable performance of the PVCEA GPE-based battery over conventional LE-based batteries. This outstanding cycling performance is reasonably explained by the fact that the crosslinked PVCEA (closely integrated into the electrodes) is less polarized than LE while suppressing dissolution of transition-metal ions from the cathode [87–90]. Therefore, it is firmly believed that the combination of radiation-sensitive precursor formulations and high-energy EB processing (compatible with the existing LIB process currently operated in battery production lines) can be considered a promising solution for the mass production of high-performance and safe solid-like GPE-based LIBs.

4. Conclusion

In conclusion, the in-situ formation of crosslinked PVCEA GPEs in fully-assembled metallic housing LIBs (capable of excellent electrochemical performance) was successfully demonstrated by high-energy (10 MeV) electron beam (EB) irradiation in a short time of less than one minute without any initiator or thermal treatment. Outstanding properties of the PVCEA, including robustness, thermal stability, desirable electrochemical properties, and good ability to hold LE, compared to the commercially used LE(Celgard) can be achieved at absorbed doses above 16 kGy and a VC:CEA molar ratio of 5:5. These superior properties are attributed to the formation of crosslinked GPEs (within the nonwoven fabric OCP) with larger occupying ionic transport volume. From the FE-SEM, EDS, and EIS analytic results for the in-situ formation of PVCEA GPEs into the NCM523/graphite full coin-type battery by EB irradiation, it was confirmed that an intimately-integrated cross-linked PVCEA GPE with both electrodes was generated, and a higher dose than 16 kGy was required for stable charge and discharge cycling capability without parasitic reactions. As a result, the PVCEA-GPE(5:5)-16-based LIB fabricated at the optimized dose of 16 kGy showed good rate capability and high discharge capacity and retention (129.2 mAh/g, >80 %, at 0.5C) after 300 cycles at 25 ℃ (corresponding to the cycling tolerant limit of the commercially available cathode (loading amount of active materials = 12 mg/cm^2) used in this study), equivalent to those from the LE(OCP)-based LIB. In particular, with regard to cycling stability at elevated temperature (60 ℃), the PVCEA(5:5)-16 GPE-based LIB was found to be more durable than the LE(OCP)-based battery due to the formation of the crosslinked PVCEA GPE even inside the electrodes. Therefore, these findings clearly verify that this fast and reliable EB processing strategy (compatible with current production lines) in combination with various organic or organic–inorganic hybrid precursor formulations is a very promising method for the industrial production of safe, cost-effective, and long-lasting in-situ gel and solid electrolyte-based LIBs.

Declaration of Competing Interest

The authors declare that they have no known competing financial interests or personal relationships that could have appeared to influence the work reported in this paper.

Data availability

No data was used for the research described in the article.

Acknowledgements

This work was supported by Korea Atomic Energy Research Institute (KAERI) Institutional Program (Project No. 523230-22).

Appendix A. Supplementary data

Supplementary data to this article can be found online at https://doi.org/10.1016/j.cej.2022.139339.

References

[1] G. Zubi, R. Dufo-López, M. Carvalho, G. Pasaoglu, The lithium-ion battery: State of the art and future perspectives, Renew. Sustain. Energy Rev. 89 (2018) 292–308, https://doi.org/10.1016/j.rser.2018.03.002.
[2] Y. Chen, Y. Kang, Y. Zhao, L. Wang, J. Liu, Y. Li, Z. Liang, X. He, X. Li, N. Tavajohi, B. Li, A review of lithium-ion battery safety concerns: the issues, strategies, and testing standards, J. Energy Chem. 59 (2021) 83–99, https://doi.org/10.1016/j.jechem.2020.10.017.
[3] K. Liu, Y. Liu, D. Lin, A. Pei, Y. Cui, Materials for lithium-ion battery safety, Sci. Adv. 4 (2018) eaas9820. https://doi.org10.1126/sciadv.aas9820.
[4] J. Duan, X. Tang, H. Dai, Y. Yang, W. Wu, X. Wei, Y. Huang, Building safe lithium-ion batteries for electric vehicles: a review, Electrochem. Energy Rev. 3 (2020) 1–42, https://doi.org/10.1007/s41918-019-00060-4.
[5] K.-S. Chen, I. Balla, N.S. Luu, M.C. Hersam, Emerging opportunities for two-dimensional materials in lithium-ion batteries, ACS Energy Lett. 2 (2017) 2026–2034, https://doi.org/10.1021/acsenergylett.7b00476.
[6] R. Schmuch, R. Wagner, G. Hörpel, T. Placke, M. Winter, Performance and cost of materials for lithium-based rechargeable automotive batteries, Nat. Energy 3 (2018) 267–278, https://doi.org/10.1038/s41560-018-0107-2.
[7] K. Xu, Electrolytes and interphases in li-ion batteries and beyond, Chem. Rev. 114 (2014) 11503–11618, https://doi.org/10.1021/cr500003w.
[8] Q. Li, J. Chen, L. Fan, X. Kong, Y. Lu, Progress in electrolytes for rechargeable Li-based batteries and beyond, Green, Energy Environ. 1 (2016) 18–42, https://doi.org/10.1016/j.gee.2016.04.006.
[9] X. Cheng, J. Pan, Y. Zhao, M. Liao, H. Peng, Gel polymer electrolytes for electrochemical energy storage, Adv. Energy Mater. 8 (2018) 1702184, https://doi.org/10.1002/aenm.201702184.
[10] J. Kalhoff, G.G. Eshetu, D. Bresser, S. Passerini, Safer electrolytes for lithium-ion batteries: state of the art and perspectives, ChemSusChem 8 (2015) 2154–2175, https://doi.org/10.1002/cssc.201500284.

[11] Q. Wang, L. Jiang, Y. Yu, J. Sun, Progress of enhancing the safety of lithium ion battery from the electrolyte aspect, Nano Energy 55 (2019) 93–114, https://doi.org/10.1016/j.nanoen.2018.10.035.

[12] M. Yuan, K. Liu, Rational design on separators and liquid electrolytes for safer lithium-ion batteries, J. Energy Chem. 43 (2020) 58–70, https://doi.org/10.1016/j.jechem.2019.08.008.

[13] W.H. Meyer, Polymer electrolytes for lithium-ion batteries, Adv. Mater. 10 (1998) 439–448, https://doi.org/10.1002/(SICI)1521-4095(199804)10:6<439::AID-ADMA439>3.0.CO;2-I.

[14] A. Arya, A.L. Sharma, Polymer electrolytes for lithium ion batteries: a critical study, Ionics 23 (2017) 497–540, https://doi.org/10.1007/s11581-016-1908-6.

[15] L. Yue, J. Ma, J. Zhang, J. Zhao, S. Dong, Z. Liu, G. Cui, L. Chen, All solid-state polymer electrolytes for high-performance lithium ion batteries, Energy Storage Mater. 5 (2016) 139–164, https://doi.org/10.1016/j.ensm.2016.07.003.

[16] Y. Wang, W.H. Zhong, Development of electrolytes towards achieving safe and high-performance energy-storage devices: a review, ChemElectroChem 2 (2015) 22–36, https://doi.org/10.1002/celc.201402277.

[17] M. Zhu, J. Wu, Y. Wang, M. Song, L. Long, S.H. Siyal, X. Yang, G. Sui, Recent advances in gel polymer electrolyte for high-performance lithium batteries, J. Energy Chem. 37 (2019) 126–142, https://doi.org/10.1016/j.jpowsour.2012.09.098.

[18] F. Baskoro, H.Q. Wong, H.J. Yen, Strategic structural design of a gel polymer electrolyte toward a high efficiency lithium-ion battery, ACS Appl. Energy Mater. 2 (2019) 3937–3971, https://doi.org/10.1021/acsaem.9b00295.

[19] A.M. Stephan, Review on gel polymer electrolytes for lithium batteries, Eur. Polym. J. 42 (2006) 21–42, https://doi.org/10.1016/j.eurpolymj.2005.09.017.

[20] S. Liang, W. Yan, X. Wu, Y. Zhang, Y. Zhu, H. Wang, Y. Wu, Gel polymer electrolytes for lithium ion batteries: Fabrication, characterization and performance, Solid State Ionics 318 (2018) 2–18, https://doi.org/10.1016/j.ssi.2017.12.023.

[21] S. Dong, N. Lv, Y. Wu, G. Zhu, X. Dong, Lithium-Ion and sodium-Ion hybrid capacitors: from insertion-type materials design to devices construction, Adv. Funct. Mater. 31 (2021) 2100455, https://doi.org/10.1002/adfm.202100455.

[22] C. Li, X. Zhang, K. Wang, X. Sun, Y. Xu, F. Su, C.-M. Chen, F. Liu, Z.-S. Wu, Y. Ma, Nitrogen-enriched graphene framework from a large-scale magnesiothermic conversion of CO_2 with synergistic kinetics for high-power lithium-ion capacitors, NPG Asia Mater. 13 (2021) 59, https://doi.org/10.1038/s41427-021-00327-7.

[23] C. Li, X. Zhang, K. Wang, F. Su, C.-M. Chen, F. Liu, Z.S. Wu, Y. Ma, Recent advances in carbon nanostructures prepared from carbon dioxide for high-performance supercapacitors, J. Energy Chem. 54 (2021) 352–367, https://doi.org/10.1016/j.jechem.2020.05.058.

[24] C. Li, X. Zhang, K. Wang, X. Sun, Y. Ma, Magnesiothermic sequestration of CO_2 into carbon nanomaterials for electrochemical energy storage: A mini review, Electrochem. Commun. 30 (2021), 107109, https://doi.org/10.1016/j.elecom.2021.107109.

[25] Y.-G. Cho, C. Hwang, D.S. Cheong, Y.-S. Kim, H.-K. Song, Gel/solid polymer electrolytes characterized by in situ gelation or polymerization for electrochemical energy systems, Adv. Mater. 31 (2019) 1804909, https://doi.org/10.1002/adma.201804909.

[26] C. Ma, W. Cui, X. Liu, Y. Ding, Y. Wang, In situ preparation of gel polymer electrolyte for lithium batteries: Progress and perspectives, InfoMat. 4 (2022) e12232.

[27] V. Vijayakumar, B. Anothumakkool, S. Kurungot, M. Winter, J.R. Nair, In situ polymerization process: an essential design tool for lithium polymer batteries, Energy Environ. Sci. 14 (2021) 2708–2788, https://doi.org/10.1039/d0ee03527k.

[28] T. Liu, J. Zhang, W. Han, J. Zhang, G. Ding, S. Dong, G. Cui, In situ polymerization for integration and interfacial protection towards solid state lithium batteries, J. Electrochem. Soc. 167 (2020), 070527, https://doi.org/10.1149/1945-7111/ab76a4.

[29] C. Li, X. Zhang, Z. Lv, K. Wang, X. Sun, X. Chen, Y. Ma, Scalable combustion synthesis of graphene-welded activated carbon for high-performance supercapacitors, Chem. Eng. J. 414 (2021), 128781, https://doi.org/10.1016/j.cej.2021.128781.

[30] W. Fan, N.-W. Li, X. Zhang, S. Zhao, R. Cao, Y. Yin, Y. Xing, J. Wang, Y.-G. Guo, C. Li, A dual-salt gel polymer electrolyte with 3D cross-linked polymer network for dendrite-free lithium metal batteries, Adv. Sci. 5 (2018) 1800559, https://doi.org/10.1002/advs.201800559.

[31] A. Hosseinioun, E. Paillard, In situ crosslinked PMMA gel electrolyte from a low viscosity precursor solution for cost-effective, long lasting and sustainable lithium-ion batteries, J. Membr. Sci. 594 (2020), 117456, https://doi.org/10.1016/j.memsci.2019.117456.

[32] M. Liu, Y. Wang, M. Li, G. Li, B. Li, S. Zhang, H. Ming, J. Qiu, J. Chen, P. Zhao, A new composite gel polymer electrolyte based on matrix of PEGDA with high ionic conductivity for lithium-ion batteries, Electrochim. Acta 354 (2020), 136622, https://doi.org/10.1016/j.electacta.2020.136622.

[33] S. Wu, H. Zheng, R. Tian, Z. Hei, H. Liu, H. Duan, In-situ preparation of gel polymer electrolyte with glass fiber membrane for lithium batteries, J. Power Sources 472 (2020), 228627, https://doi.org/10.1016/j.jpowsour.2020.228627.

[34] J. Jeong, H. Lee, J. Choi, M.-H. Ryou, Y.M. Lee, Effect of $LiFePO_4$ cathode density and thickness on electrochemical performance of lithium metal polymer batteries prepared by in situ thermal polymerization, Electrochim. Acta 154 (2020) 149–156, https://doi.org/10.1016/j.electacta.2014.12.051.

[35] M. Liu, S. Zhang, G. Li, C. Wang, B. Li, M. Li, Y. Wang, B. Li, M. Li, Y. Wang, H. Ming, Y. Wen, J. Qiu, J. Chen, P. Zhao, A cross-linked gel polymer electrolyte employing cellulose acetate matrix and layered boron nitride filler prepared via in situ thermal polymerization, J. Power Sources 484 (2021), 229235, https://doi.org/10.1016/j.jpowsour.2020.229235.

[36] X. Li, K. Qian, Y.-B. He, C. Liu, D. An, Y. Li, D. Zhou, Z. Lin, B. Li, Q.-H. Yang, F. Kang, A dual-functional gel-polymer electrolyte for lithium ion batteries with superior rate and safety performances, J. Mater. Chem. A 5 (2017) 18888–18895, https://doi.org/10.1039/c7ta04415a.

[37] Q. Wang, X. Xu, B. Hong, M. Bai, J. Li, Z. Zhang, Y. Lai, Molecular engineering of a gel polymer electrolyte via in-situ polymerization for high performance lithium metal batteries, Chem. Eng. J. 428 (2022), 131331, https://doi.org/10.1016/j.cej.2021.131331.

[38] D. Zhou, D. Shanmukaraj, A. Tkacheva, M. Armand, G. Wang, Polymer electrolytes for lithium-based batteries: advances and prospects, Chem 5 (2019) 2326–2352, https://doi.org/10.1016/j.chempr.2019.05.009.

[39] J.-T. Lee, M.-S. Wu, F.-M. Wang, H.-W. Liao, C.-C. Li, S.-M. Chang, C.-R. Yang, Gel polymer electrolytes prepared by in situ atom transfer radical polymerization at ambient temperature, Electrochem. Solid-State Lett. 10 (4) (2007) A97–A100, https://doi.org/10.1149/1.2435510.

[40] H. Guan, F. Lian, K. Xi, Y. Ren, J. Sun, R.V. Kumar, Polyvinyl formal based gel polymer electrolyte prepared using initiator free in-situ thermal polymerization method, J. Power Sources 245 (2014) 95–100, https://doi.org/10.1016/j.jpowsour.2013.06.120.

[41] S.S. Hwang, C.G. Cho, H. Kim, Room temperature cross-linkable gel polymer electrolytes for lithium ion batteries by in situ cationic polymerization of divinyl ether, Electrochem. Commun. 12 (2010) 916–919, https://doi.org/10.1016/j.elecom.2010.04.020.

[42] Y. Cui, J. Chai, H. Du, Y. Duan, G. Xie, Z. Liu, G. Cui, Facile and reliable in situ polymerization of poly(ethyl cyanoacrylate)-based polymer electrolytes toward flexible lithium batteries, ACS Appl. Mater. Interfaces 9 (2017) 8737–8741, https://doi.org/10.1021/acsami.6b16218.

[43] F.-Q. Liu, W.-P. Wang, Y.-X. Yin, S.-F. Zhang, J.-L. Shi, L. Wang, X.-D. Zhang, Y. Zheng, J.-J. Zhou, L. Li1, Y.-G. Guo,, Upgrading traditional liquid electrolyte via in situ gelation for future lithium metal batteries, Sci. Adv. 4 (2018) eaat5383, https://doi.org/10.1126/sciadv.aat5383.

[44] Q. Zhao, X. Liu, S. Stalin, K. Khan, L.A. Archer, Solid-state polymer electrolytes with in-built fast interfacial transport for secondary lithium batteries, Nat. Energy 4 (2019) 365–373, https://doi.org/10.1038/s41560-019-0349-7.

[45] S. Huang, Z. Cui, L. Qiao, G. Xu, J. Zhang, K. Tang, X. Liu, Q. Wang, X. Zhou, B. Zhang, G. Cui, An in-situ polymerized solid polymer electrolyte enables excellent interfacial compatibility in lithium batteries, Electrochim. Acta 299 (2019) 820–827, https://doi.org/10.1016/j.electacta.2019.01.039.

[46] W.-P. Wang, J. Zhang, Y.-X. Yin, H. Duan, J. Chou, S.-Y. Li, M. Yan, S. Xin, Y.-G. Guo, A rational reconfiguration of electrolyte for high-energy and long-life lithium–chalcogen batteries, Adv. Mater. 32 (2020) 2000302, https://doi.org/10.1002/adma.202000302.

[47] S. Wang, L. Zhou, M.K. Tufail, L. Yang, P. Zhai, R. Chen, W. Yang, In-situ synthesized non-flammable gel polymer electrolyte enable highly safe and dendrite-Free lithium metal batteries, Chem. Eng. J. 415 (2021), 128846, https://doi.org/10.1016/j.cej.2021.128846.

[48] H. Cheng, J. Zhu, H. Jin, C. Gao, H. Liu, N. Cai, Y. Liu, P. Zhang, M. Wang, In situ initiator-free gelation of highly concentrated lithium bis(fluorosulfonyl)imide-1,3-dioxolane solid polymer electrolyte for high performance lithium-metal batteries, Mater. Today Energy 20 (2021), 100623, https://doi.org/10.1016/j.mtener.2020.100623.

[49] M. Tamada, Radiation processing of polymers and its applications, in: H. Kudo (Ed.), Radiation Applications, Springer, Singapore, 2018, pp. 63–80, https://doi.org/10.1007/978-981-10-7350-2_8.

[50] A.T. Naikwadi, B.K. Sharma, K.D. Bhatt, P.A. Mahanwar, Gamma radiation processed polymeric materials for high performance applications: a review, Front. Chem. 10 (2022), 837111, https://doi.org/10.3389/fchem.2022.837111.

[51] T.A. Elmaaty, S. Okubayashi, H. Elsisi, S. Abouelenin, Electron beam irradiation treatment of textiles materials: a review, J. Polym. Res. 29 (2022) 117, https://doi.org/10.1007/s10965-022-02952-4.

[52] D.L. Wood III, M. Wood, J. Li, Z. Du, R.E. Ruther, K.A. Hays, N. Muralidharan, L. Geng, C. Mao, I. Belharouak, Perspectives on the relationship between materials chemistry and roll-to-roll electrode manufacturing for high-energy lithium-ion batteries, Energy Storage Mater. 29 (2020) 254–265, https://doi.org/10.1016/j.ensm.2020.04.036.

[53] Y.F. Zhou, S. Xie, X.W. Ge, C.H. Chen, K. Amine, Preparation of rechargeable lithium batteries with poly(methyl methacrylate) based gel polymer electrolyte by in situ γ-ray irradiation-induced polymerization, J. Appl. Electrochem. 34 (2004) 1119–1125, https://doi.org/10.1007/s10800-004-2726-5.

[54] Y. Wang, J. Qiu, J. Peng, J. Li, M. Zhai, One-step radiation synthesis of gel polymer electrolytes with high ionic conductivity for lithium-ion batteries, J. Mater. Chem. A 5 (2017) 12393–12399, https://doi.org/10.1039/c7ta02291c.

[55] M. Sun, Z. Zeng, W. Hu, K. Sheng, Z. Wang, Z. Han, L. Peng, C. Yu, S. Cheng, M. Fan, J. Huang, J. Xie, Scalable fabrication of solid-state batteries through high-energy electronic beam, Chem. Eng. J. 431 (2022), 134323, https://doi.org/10.1016/j.cej.2021.134323.

[56] M.R. Cleland, L.A. Parks, Medium and high-energy electron beam radiation processing equipment for commercial applications, Nucl. Instrum. Methods Phys. Res., Sect. B 208 (2003) 74-89. https://doi.org/10.1016/S0168-583X(03)00672-4.

[57] D. Gheysari, A. Behjat, Radiation crosslinking of LDPE and HDPE with 5 and 10 MeV electron beams, Eur. Polym. J. 37 (2001) 2011–2016, https://doi.org/10.1016/S0014-3057(01)00084-2.

[58] M.G. Golkovski, I.A. Bataev, A.A. Bataev, A.A. Ruktuev, T.V. Zhuravina, N. K. Kuksanov, R.A. Salimov, V.A. Bataev, Atmospheric electron-beam surface

alloying of titanium with tantalum, Mater. Sci. Eng. A 578 (2013) 310–317, https://doi.org/10.1016/j.msea.2013.04.103.
[59] D. Ticoş, M. Galaţanu, A. Galaţanu, M. Dumitru, M.L. Mitu, N. Udrea, A. Scurtu, C. M. Ticoş, Irradiation of W and K-Doped W Laminates without or with Cu, V, Ti Interlayers under a Pulsed 6 MeV Electron Beam, Materials 15 (2022) 956, https://doi.org/10.3390/ma15030956.
[60] J. Chai, Z. Liu, J. Zhang, J. Sun, Z. Tian, Y. Ji, K. Tang, X. Zhou, G. Cui, A superior polymer electrolyte with rigid cyclic carbonate backbone for rechargeable lithium ion batteries, ACS Appl. Mater. Interfaces 9 (2017) 17897–17905, https://doi.org/10.1039/c7ra00112f.
[61] T. Dong, H. Zhang, R. Hu, P. Mu, Z. Liu, X. Du, C. Lu, G. Lu, W. Liu, G. Cui, A rigid-flexible coupling poly (vinylene carbonate) based cross-linked network: A versatile polymer platform for solid-state polymer lithium batteries, Energy Storage Mater. 50 (2022) 525–532, https://doi.org/10.1016/j.ensm.2022.05.052.
[62] K.I.S. Mongcopa, D.A. Gribble, W.S. Loo, M. Tyagi, S.A. Mullin, N.P. Balsara, Segmental dynamics measured by quasi-Elastic neutron scattering and ion transport in chemically distinct polymer electrolytes, Macromolecules 53 (2020) 2406–2411, https://doi.org/10.1021/acs.macromol.0c00091.
[63] Z. Lv, Q. Zhou, S. Zhang, S. Dong, Q. Wang, L. Huang, K. Chen, G. Cui, Cyano-reinforced in-situ polymer electrolyte enabling long-life cycling for high-voltage lithium metal batteries, Energy Storage Mater. 37 (2021) 215–223, https://doi.org/10.1016/j.ensm.2021.01.017.
[64] D.-H. Kim, S. Hwang, J.-J. Cho, S. Yu, S. Kim, J. Jeon, K.H. Ahn, C. Lee, H.-K. Song, H. Lee, Toward fast operation of lithium batteries: ion activity as the factor to determine the concentration polarization, ACS Energy Lett. 4 (2019) 1265–1270, https://doi.org/10.1021/acsenergylett.9b00724.
[65] T. Zhou, Y. Zhao, J.W. Choi, A. Coskun, Ionic liquid functionalized gel polymer electrolytes for stable lithium metal batteries, Angew. Chem. 133 (2021) 22973–22978, https://doi.org/10.1002/ange.202106237.
[66] J.-K. Kim, D.H. Kim, S.H. Joo, B. Choi, A. Cha, K.M. Kim, T.-H. Kwon, S.K. Kwak, S. J. Kang, J. Jin, Hierarchical chitin fibers with aligned nanofibrillar architectures: a nonwoven-mat separator for lithium metal batteries, ACS Nano 11 (2017) 6114–6121, https://doi.org/10.1021/acsnano.7b02085.
[67] X. Leng, M. Yang, C. Li, W.U. Arifeen, T.J. Ko, High-performance separator for lithium-ion battery based on dual-hybridizing of materials and processes, Chem. Eng. J. 433 (2022), 133773, https://doi.org/10.1016/j.cej.2021.133773.
[68] A. Ashfaq, M.-C. Clochard, X. Coqueret, C. Dispenza, M.S. Driscoll, P. Ulański, M. Al-Sheikhly, Polymerization reactions and modifications of polymers by ionizing radiation, Polymers 12 (2020) 2877, https://doi.org/10.3390/polym12122877.
[69] M. Ferry, Y. Ngono, Energy transfer in polymers submitted to ionizing radiation: A review, Radiat. Phys. Chem. 180 (2021), 109320, https://doi.org/10.1016/j.radphyschem.2020.109320.
[70] J. Ju, Y. Wang, B. Chen, J. Ma, S. Dong, J. Chai, H. Qu, L. Cui, X. Wu, G. Cui, Integrated interface strategy toward room temperature solid-state lithium batteries, ACS Appl. Mater. Interfaces 10 (2018) 13588–13597, https://doi.org/10.1021/acsami.8b02240.
[71] C. Niu, M. Zhang, G. Chen, B. Cao, J. Shi, J. Du, Y. Chen, An effectively inhibiting lithium dendrite growth in-situ-polymerized gel polymer electrolyte, Electrochim. Acta 283 (2018) 349–356, https://doi.org/10.1016/j.electacta.2018.06.169.
[72] J. Ma, Q. Dai, X. Li, X. Zhu, T. Ma, X. Qiao, S. Shen, X. Liu, Dipentaerythritol penta-/hexa-acrylate based-highly cross-linked hybrid monolithic column: Preparation and its applications for ultrahigh efficiency separation of proteins, Anal. Chim. Acta 963 (2017) 143–152, https://doi.org/10.1016/j.aca.2017.01.057.
[73] D.M. Seo, S. Reininger, M. Kutcher, K. Redmond, W.B. Euler, B.L. Lucht, Role of mixed solvation and ion pairing in the solution structure of lithium ion battery electrolytes, J. Phys. Chem. C 119 (2015) 14038–14046, https://doi.org/10.1021/acs.jpcc.5b03694.
[74] H. Li, X.-T. Ma, J.-L. Shi, Z.-K. Yao, B.-K. Zhu, L.-P. Zhu, Preparation and properties of poly (ethylene oxide) gel filled polypropylene separators and their corresponding gel polymer electrolytes for Li-ion batteries, Electrochim. Acta 56 (2011) 2641–2647, https://doi.org/10.1016/j.electacta.2010.12.010.
[75] Y. Tong, Y. Xu, D. Chen, Y. Xie, L. Chen, M. Que, Y. Hou, Deformable and flexible electrospun nanofiber-supported cross-linked gel polymer electrolyte membranes for high safety lithium-ion batteries, RSC adv. 7 (2017) 22728–22734, https://doi.org/10.1039/C7RA00112F.
[76] D. Xu, J. Su, J. Jin, C. Sun, Y. Ruan, C. Chen, Z. Wen, In situ generated fireproof gel polymer electrolyte with $Li_{6.4}Ga_{0.2}La_3Zr_2O_{12}$ as initiator and ion-conductive filler, Adv. Energy Mater. 9 (2019) 1900611, https://doi.org/10.1002/aenm.201900611.
[77] N. Hosoya, K. Nishiguchi, H. Saito, S. Maeda, Chemically cross-linked gel storage for fuel to realize evaporation suppression, Chem. Eng. J. 444 (2022), 136506, https://doi.org/10.1016/j.cej.2022.136506.
[78] D. Belov, D.-T. Shieh, GBL-based electrolyte for Li-ion battery: thermal and electrochemical performance, J. Solid State Electrochem. 16 (2012) 603–615, https://doi.org/10.1007/s10008-011-1391-y.
[79] L. Li, M. Wang, J. Wang, F. Ye, S. Wang, Y. Xu, J. Liu, G. Xu, Y. Zhang, Y. Zhang, C. Yan, N.V. Medhekar, M. Liu, Y. Zhang, Asymmetric gel polymer electrolyte with high lithium ion conductivity for dendrite-free lithium metal batteries, J. Mater. Chem. A 8 (2020) 8033–8040, https://doi.org/10.1039/d0ta01883j.
[80] D. Zhou, L.-Z. Fan, H. Fan, Q. Shi, Electrochemical performance of trimethylolpropane trimethylacrylate-based gel polymer electrolyte prepared by in situ thermal polymerization, Electrochim. Acta 89 (2013) 334–338, https://doi.org/10.1016/j.electacta.2012.11.090.
[81] Y. Wang, L. Fu, L. Shi, Z. Wang, J. Zhu, Y. Zhao, S. Yuan, Gel polymer electrolyte with high Li^+ transference number enhancing the cycling stability of lithium anodes, ACS Appl. Mater. Interfaces 11 (2019) 5168–5175, https://doi.org/10.1021/acsami.8b21352.
[82] P. Wang, J. Chai, Z. Zhang, H. Zhang, Y. Ma, G. Xu, H. Du, T. Liu, G. Li, G. Cui, An intricately designed poly(vinylene carbonate-acrylonitrile) copolymer electrolyte enables 5 V lithium batteries, J. Mater. Chem. A 7 (2019) 5295–5304, https://doi.org/10.1039/c9ta00204a.
[83] Z. Li, Y. Zhao, W.E. Tenhaeff, 5 V stable nitrile-bearing polymer electrolyte with aliphatic segment as internal plasticizer, ACS Appl. Energy Mater. 2 (2019) 3264–3273, https://doi.org/10.1021/acsaem.9b0010.
[84] S. Chen, H. Che, F. Feng, J. Liao, H. Wang, Y. Yin, Z.-F. Ma, Poly(vinylene carbonate)-based composite polymer electrolyte with enhanced interfacial stability to realize high-performance roomtemperature solid-state sodium batteries, ACS Appl. Mater. Interfaces 11 (2019) 43056–43065, https://doi.org/10.1021/acsami.9b11259.
[85] H. Ogawa, H. Mori, In-situ formation of poly(ionic liquid)s with ionic liquid-based plasticizer and lithium salt in electrodes for solid-state lithium batteries, Polymer 178 (2019), 121614, https://doi.org/10.1016/j.polymer.2019.121614.
[86] K.-H. Lee, H.S. Lim, J.H. Wang, Effect of unreacted monomer on performance of lithium-ion polymer batteries based on polymer electrolytes prepared by free radical polymerization, J. Power Sources 139 (2005) 284–288, https://doi.org/10.1016/j.jpowsour.2004.07.007.
[87] T. Chen, Y. Liao, L. Yang, X. Li, W. Li, Improved performance of $LiNi_{0.5}Mn_{1.5}O_4$ cathode for high-voltage lithium-ion battery at elevated temperature by using gel polymer electrolyte, Ionics 21 (2015) 2457–2463, https://doi.org/10.1007/s11581-015-1424-0.
[88] J. Zheng, Y. Zhao, X. Feng, W. Chen, Y. Zhao, Novel safer phosphonate-based gel polymer electrolytes for sodium-ion batteries with excellent cycling performance, J. Mater. Chem. A 6 (2018) 6559–6564, https://doi.org/10.1039/c8ta00530c.
[89] Y.-G. Cho, S.H. Jung, J. Jeong, H. Cha, K. Baek, J. Sung, M. Kim, H.T. Lee, H. Kong, J. Cho, S.J. Kang, J.M. Park, H.-K. Song, Metal-ion chelating gel polymer electrolyte for Ni-rich layered cathode materials at a high voltage and an elevated temperature, ACS Appl. Mater. Interfaces 13 (2021) 9965–9974, https://doi.org/10.1021/acsami.0c21164.
[90] H.M.K. Sari, X. Li, Controllable cathode–electrolyte interface of $Li[Ni_{0.8}Co_{0.1}Mn_{0.1}]O_2$ for lithium ion batteries: A review, Adv. Energy Mater. 9 (2019) 1901597, https://doi.org/10.1002/aenm.201901597.